Biotribology 12 (2017) 52–58

Contents lists available at ScienceDirect

Biotribology

journal homepage: www.elsevier.com/locate/biotri

New Non-invasive Techniques to Quantify Skin Surface Strain and Sub-surface Layer Deformation of Finger-pad during Sliding

X. Liu[a,c,1], R. Maiti[a,*,1], Z.H. Lu[b], M.J. Carré[a], S.J. Matcher[b], R. Lewis[a]

[a] Department of Mechanical Engineering, Sir Frederick Mappin Building, University of Sheffield, UK
[b] Department of Electronic and Electrical, University of Sheffield, UK
[c] General Engineering and Research Institute, Liverpool John Moors University, Byrom Street, Liverpool L3 3AF, UK

ARTICLE INFO

Keywords:
Sliding
Optical coherence tomography
Digital image correlation
Finger-pad

ABSTRACT

Studies on the variation of skin properties with gender, age and anatomical region, with regards to interaction with different materials have resulted in significant research output. Investigations on skin surface strain and sub-surface layer deformation during sliding, however, have not received as much attention. This novel study uses two non-invasive techniques, optical coherence tomography (OCT) and digital image correlation (DIC), to measure properties of the index finger of a 25 year old female when under normal and shear loading. Measurements were taken during static, and for the first time, dynamic phases.

It was observed that the number of ridges in contact with a Quartz glass surface, observed under OCT, reduced when the finger started sliding. The sliding also resulted in deformation at the stratum corneum junction. The surface strain, analysed using DIC was higher nearer to the distal interphalangeal joint compared to the fingertip. This newly developed approach provides a powerful and non-invasive method to study the structural changes of finger-pad skin during loading and sliding. This approach can now be repeated at different anatomical locations for medical, bioengineering and consumer applications.

1. Introduction

Skin is the largest organ in human body and the first line of protection against all interactions and potential damage. There are three main layers in adult skin: the hypodermis, dermis and epidermis, with total thickness varying from 0.5 mm to 6 mm [1,2]. This study is concerned with the epidermis, which consists of five sub layers, namely stratum basale, stratum spinosum, stratum granulosum, stratum lucidum and stratum corneum [3].

1.1. General Overview

There is significant variation in skin properties for different ages, genders and body regions due to variations in tissue thickness and anatomical differences [4–6]. The presence of hair follicles, for example, alters the visco-elastic properties of the skin and subcutaneous tissues [7]. Not a great deal is known about the mechanisms behind the behaviour of finger-pad skin when interacting with external materials even though it has been the subject of much interest due to its importance in daily living (grip and explorative touch), health and consumer products. Knowledge on contact mechanics and frictional behaviour of the finger-pad is essential to improve the surface interactions with the materials coming into physical contact. However, finger-pad skin behaves differently between subjects, loading conditions and environment resulting in comparative difficulties in the past studies [7]. The difference may be caused due to variation of thickness, geometry, roughness, melanin and erythema content between different subjects.

Various tribological devices have been used to measure the friction between skin and materials such as metal, rubber and polymer, showing the different effects caused by material roughness [7–9], moisture [7,10–14], roughness [7–11,13] and loading [7–9,11–13]. Force plates have been widely used to measure the friction caused by dragging a finger-pad across a material sample under applied loads [7–9,12].

1.2. Skin Strain Measurement

Digital image correlation (DIC) and optical coherence tomography (OCT) are non-invasive techniques only used relatively recently to examine skin tissue behaviour during loading at the surface [15–18] and sub-surface [19–21]. To our knowledge, only a few investigations [22–24] have focussed on quantifying the structural change in finger-

* Corresponding author.
E-mail address: r.maiti@sheffield.ac.uk (R. Maiti).
[1] X. Liu and R. Maiti have contributed equally.

http://dx.doi.org/10.1016/j.biotri.2017.07.001
Received 21 November 2016; Received in revised form 12 July 2017; Accepted 17 July 2017
Available online 18 July 2017

pad during sliding. Delhaye et al. [23] investigated finger-pad surface strain on 8 volunteers. They observed that the strain patterns propagated from periphery to the centre of the contact area during sliding. In addition, a few authors [14,24–25] also investigated on the changes to contact area during sliding. Understanding the deformation of the skin during sliding, where the interface includes stick and slip regions [13–14,24–25], will provide additional insight of the finger-pad friction mechanism.

All the authors listed above have investigated on the effect of friction during sliding on the surface of finger-tip reporting the effect of type of interacting materials, roughness, load and moisture on the finger-pad skin. None, have investigated the deformation of sub-surface layers during sliding based on geometrical changes of deeper tissue layers. The aim of this work was to use OCT and DIC to determine the surface strain and sub-surface deformation of a finger-pad during combination of applied normal load and tangential force (shear force or sliding) to understand variation of skin properties. Understanding the strain variation in the finger surface and sub-surface under these loading scenarios, will enable enhancement of finger-tip models as simulations with more representative layer structure and behaviour can be created. This data can also be used for applications in medicine (artificial grafts design), bioengineering (sensor design) and consumer products (dexterity, touch, feel). The capability to characterise strain in skin could also help give details about the irritation and reddening of the skin. For example, wearing sensors in a hot atmosphere, can result in strain on the skin surface, has links to the formation of rashes.

2. Experimental Details

2.1. Finger-pad Imaging

2.1.1. In-House Swept-Source Optical Coherence Tomography (SS-OCT) System

Imaging of finger-pad skin was performed using a home-built SS-OCT system that is based on a Michelson Diagnostics Ltd. swept source OCT data acquisition system (Michelson Diagnostics, Kent, United Kingdom) coupled to a Thorlabs LSM03 scan lens and in-house fibre based Michelson interferometer. Fig. 1 shows a photograph and the schematic diagram of the system used.

The light source was a Santec HSL-2000-10 wide sweep-laser with a wavelength of 1305 nm ± 15 nm with a full width at half maximum (FWHM) of 110 nm. This led to an axial resolution of about 10 μm in air and 15 μm in tissue.

The light was split and coupled to the reference and the sample arms with equal power through a 2 × 2 single-mode fibre-optic coupler. In the reference arm, the light beam was reflected from an optical mirror and redirected to the coupler. The sample arm contains a two-axis galvanometer scanner (6215, Cambridge Technology, US) and the Thorlabs LSM03 OCT scanning lens, yielding a mean spot size in the focal plane of 25 μm, which also defined the system lateral scanning resolution. The light beams from the reference and the sample arms are combined at the coupler and interfere with each other, used to create an OCT image (Fig. 1c).

2.1.2. Digital Image Correlation (DIC)

DIC is an optical technique capable of providing full-field surface displacement/strain measurements. The principle behind 2D-DIC is to track the changing displacement of a speckled pattern, sprayed on the surface, due to loading and hence calculate the strain over the region measured. More details of this principle can be found in Sutton et al. [27].

The 2D-DIC system used consisted of a 5-MP AVT Pike camera (2452 × 2054 pixels), a computer and two white light sources, as shown in Fig. 2. The Pike camera is capable of high speed flash synchronisation at full resolution. The frame rate of the camera was set to 150 frame/ms.

All images were analysed using a commercial DIC software package (Vic-2D, 2007, Correlated Solutions Inc., Columbia, USA). The calculation of Lagrange's strain in X (e_{xx}) and Y (e_{yy}) axes are explained in Maiti et al. [28]. Strain plot was calculated by obtaining the values of strain from the slice corresponding to the middle of the finger. An optimised 6-tap filter was used to plot the strain data between two measured DIC stain points.

2.2. Materials and Test Apparatus

The same finger was used throughout testing; the right middle finger of a 25 year-old female. This was in contact with an optical-grade Quartz glass plate with an average surface roughness of below 0.01 μm, measured using Profilometer (Mitutyo UK Ltd), and a thickness of 1 mm.

A HE6X6 multi-axial force plate (Advanced Mechanical Technology Inc., Massachusetts, USA) was used in the study, with inbuilt force data acquisition software sampling at a rate of 25 kHz. The plate has the capacity to withstand a 44 N force in the Z axis and a 22 N force along the X and Y axes. The force plate was modified to include a raised table with the glass plate mounted, as shown in Fig. 3(a). A finger was pressed upwards (along the direction of applied normal load) from below the glass plate sliding against the glass plate as shown in Fig. 3(b). A tangential force (shear or sliding) opposite to the direction of motion is created. This arrangement allowed viewing of the contact from above, by OCT or DIC. The finger was tapped on the glass before measurements were recorded to synchronise the load and image capturing.

2.3. Test Methods and Conditions

Before each test, the participant was required to wash her hands, and dry them with paper towels. Regions on the finger were marked for OCT deformation measurement. To obtain the image deformation in DIC, the finger pad skin had random dots applied with semi-permanent ink, as shown in Fig. 4(a). In order to obtain clear images with reduced light reflectance from the top surface of the glass window, the glass plate was tilted slightly.

All experiments were conducted at a constant sliding speed of 10 ± 2 mm/s and an applied normal load of 6 ± 0.5 N. Displacement vectors (white dotted lines) across the centre of the finger pad were used to quantify the deformation in the finger pad. One hundred points were selected based on the line of analysis shown in Fig. 4(b). The area of interest was divided into axes X and Y as shown in Fig. 4(c).

Images from OCT were captured at 10 images per second during static and dynamic phases. The contact between ridges of human finger skin were plotted against the glass plate (Fig. 5) in ImageJ (Contributors Worldwide, USA). The contact perimeter was quantified by calculating the percentage ratio of total length of contact (d1 + d2 + d3 + d4 + d5) and image length (4 mm).

Images from DIC were taken at each stage of the motion to allow the strain at the finger-pad surface to be investigated. Each finger position was assigned a number, relating to its respective image (see Fig. 6). Images for positions P_0 to P_{15} relate to the pre-movement period, considered as the reference images with applied horizontal and shear loads (static phase). P_{15} defines the position of the finger on the verge of moving (static phase) when the tangential force overcomes the friction resistance and is about to start sliding i.e. shear force changes to sliding. P_{16} to P_{56} were the positions of finger during sliding (dynamic phase).

The DIC/OCT – friction experiments were repeated twice. Additional friction experiments were carried out five times to test the repeatability of the finger-pad glass interaction. The error bars of the strain plots and friction experiments were not plotted to avoid over-complicating the graphs in the result sections.

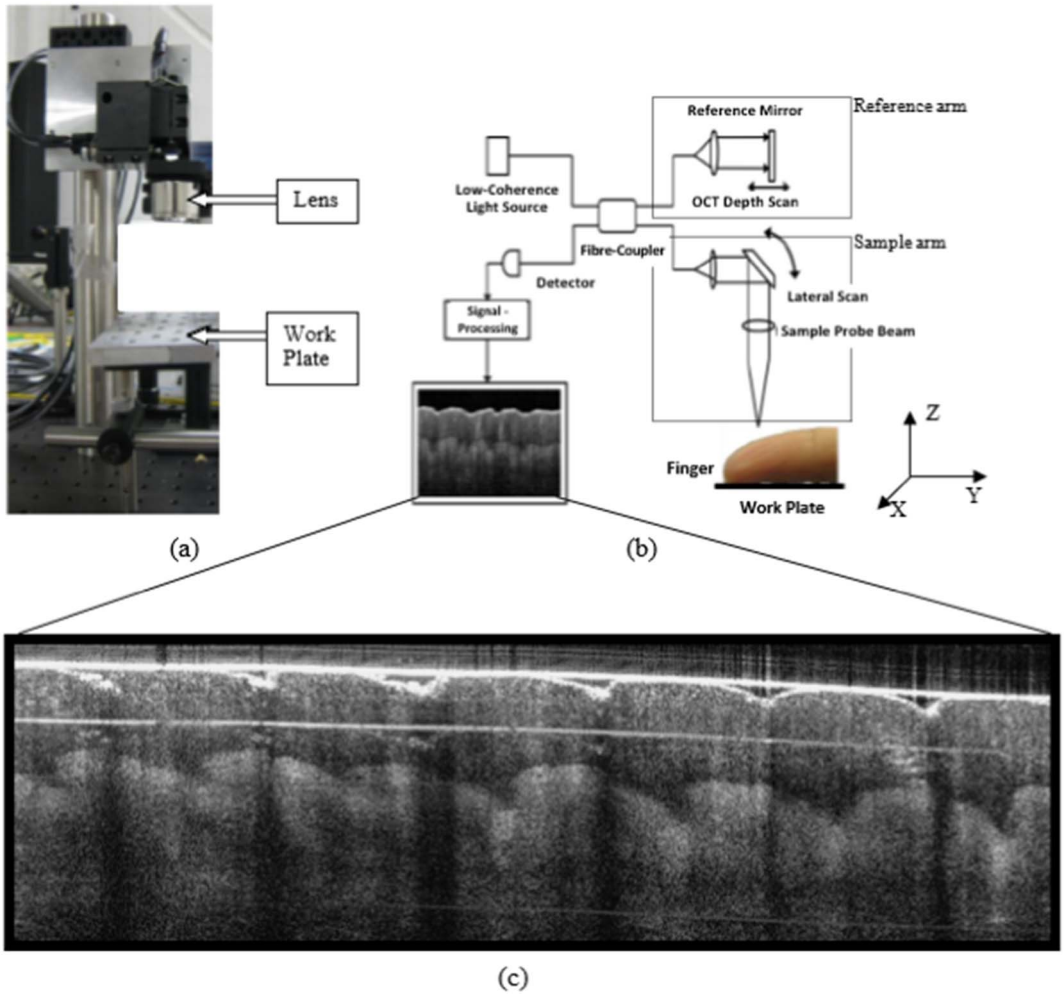

Fig. 1. (a) Photography of the SS-OCT system, (b) the schematic diagram of the system (Modified from [26]) and (c) sample OCT image.

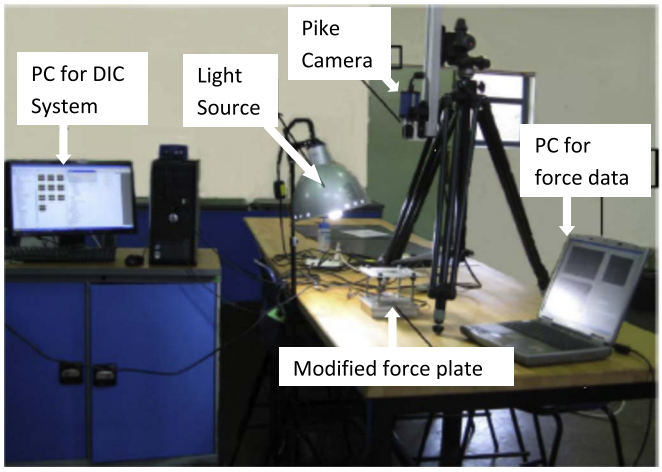

Fig. 2. Set-up for 2D DIC system.

3. Results and Discussion

3.1. Deformation of Sub Layers of Finger-pad Skin

OCT images of the finger-pad taken while in static and dynamic phases are shown in Fig. 7. During the static phase, ridges come into contact with the glass surface as shown in white dotted circles in Fig. 7(a). When the tangential force is increased beyond shear, sliding occurs i.e. dynamic phase, and the number of distinguishable ridges in the image decreases (Fig. 7(b)) as the finger contact with the glass surface becomes flat. The real contact perimeter from a single image slice (based on the average length from numerous slices) during the static phase was measured to be 50% of the total available image length (4 mm). The real contact perimeter increased from 50% to 88% of the available contact length during dynamic phase. The increased tangential force and initiation of sliding resulted in smoothening of the stratum corneum junction as shown in Fig. 7.

Skin is firmly connected to the underlying body tissue structures. When the multilayer composite is subjected to stretching due to sliding of finger-pad over glass or mechanical loading as reported in Maiti et al. [28], the skin will accommodate the exposed strain and respond in such a way that both the stratum corneum junction, in this study, flatten and top skin surface asperities smoothen out.

3.2. Strain on Finger-pad Skin Surface

Vector displacement maps of the examined region of the finger-pad are shown in Fig. 8 with the X and Y axes origin representing the lateral side of interphalangeal joint. The first image, Fig. 8(a) is during contact with a glass surface at 0.2 N pre-loading stage and shows minor deformation of the finger pad. Fig. 8(b) shows distortions in the finger as applied normal load and shear force was applied during the static phase. An increment in tangential force (beyond the limit of shear force, just before the glass plate starts sliding), necessary for sliding during the dynamic phase led to higher distortion as seen in Fig. 8(c).

Surface strain in the X axis along a mid-line was extracted and

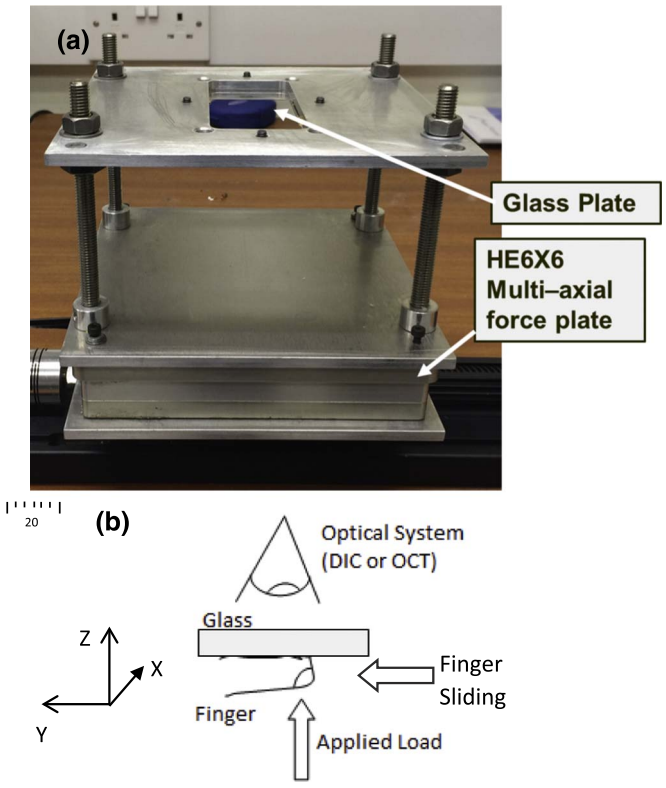

Fig. 3. The set-up of (a) Multi-axial force plate, (b) finger-glass interface.

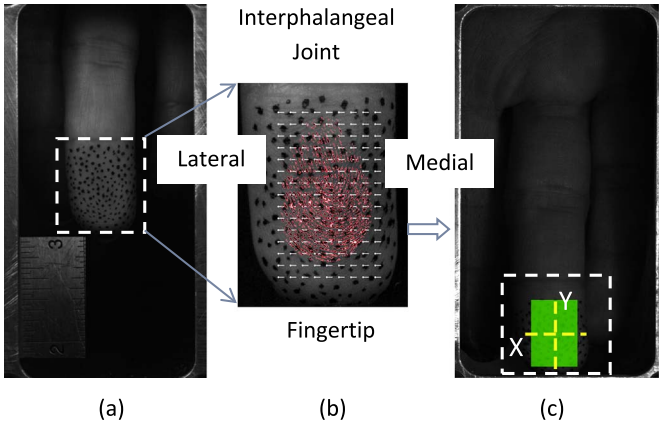

Fig. 4. DIC images of finger-pad skin (a) Ref image; (b) initial area of analysis marked with red ink; and (c) two centre lines plotted with X and Y axes.

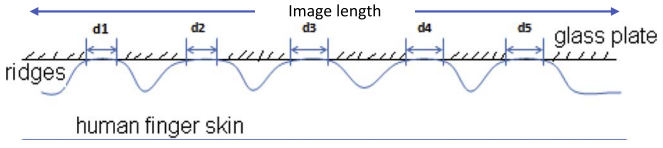

Fig. 5. Calculation of contact perimeter.

Fig. 6. Finger position represented as P0-P56 on the finger-pad surface during sliding.

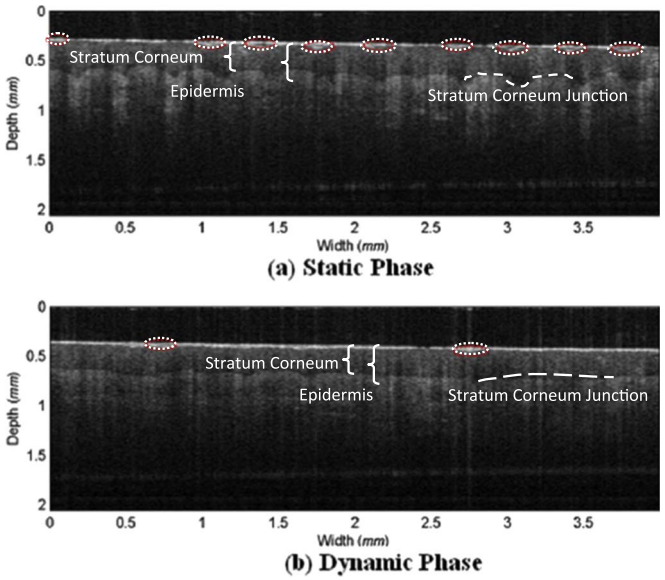

Fig. 7. OCT images of the finger-pad skin in contact with the glass surface (gap between finger-pad the surface marked by white dotted circles), obtained during (a) static phase; (b) dynamic phase of contact.

plotted in static phase (without sliding initiation) with change in load as shown in Fig. 9(a). The lower force of 0.02 N magnitude (Fig. 9b) was obtained when the force plate first registered any measurable effect of contact with the finger. The strain data fluctuates in the X direction with skin stretching along the lateral and medial edges (Fig. 9 c–e). The highest percentile change in surface strain (22%) was observed at the medial edge for about 1 N loading. The middle section of the finger-pad in the Coronal plane (dividing front/anterior and back/posterior) was rarely influenced by normal load and tangential force applied during static and dynamic phases.

The strain (e_{yy}) in the Y axis represents the local tangential strain corresponding to the friction force observed during sliding of the finger. Four different points in the friction and normal forces curve (Fig. 10a) were analysed. Point P_1 represents the point without any applied normal load and acts as a reference. P12 was selected during static phase with no sliding, but under both normal load and shear force, P16 was selected when sliding was initated and P37 was selected based on complete sliding i.e. the dynamic phase having been fully developed.

Point P_{12} corresponds to the state of maximum normal load and shear force (70% of maximum tangential force), both with magintude of 2.5 N at time 4.5 s. The surface strain measured between the finger pad and the glass surface at this stage was − 3.2% and 2.3% at the distal interphalangeal joint end and fingertip end respectively (Fig. 10(b)). Point P_{16} corresponds to the friction force (highest tangential force) during transition between the static and dynamic phases. The surface strain increased by 3.6% at the fingertip and decreased by − 11.2% in the distal interphalangeal joint. Friction force and normal load were similar at positions P_{16} and P_{37}, and therefore gave similar YY strain plots. Strain in the mid-region of the skin contact was significantly smaller (Figs. 9 and 10) with respect to the other regions. This observation was similar to that by Tada et al. [24], suggesting no

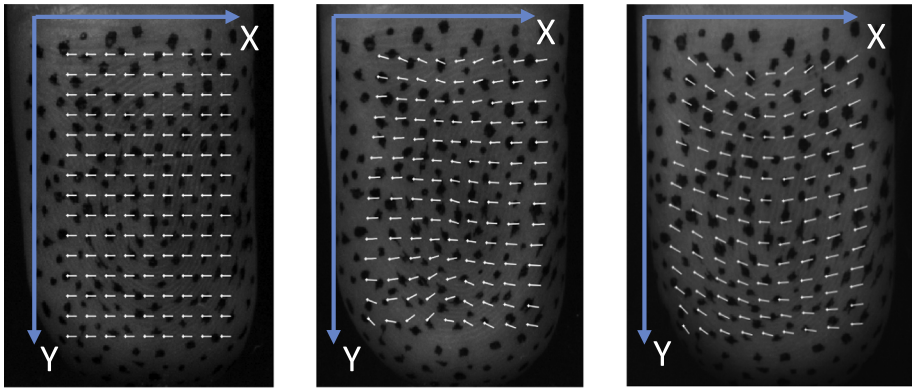

Fig. 8. Displacement field of a finger in X and Y axes (origin at lateral interphalangeal joint) corresponding to: (a) minor flattening against the glass, (b) static phase of contact with glass, without movement between interfaces but under shear loading, and (c) dynamic sliding phase with sliding.

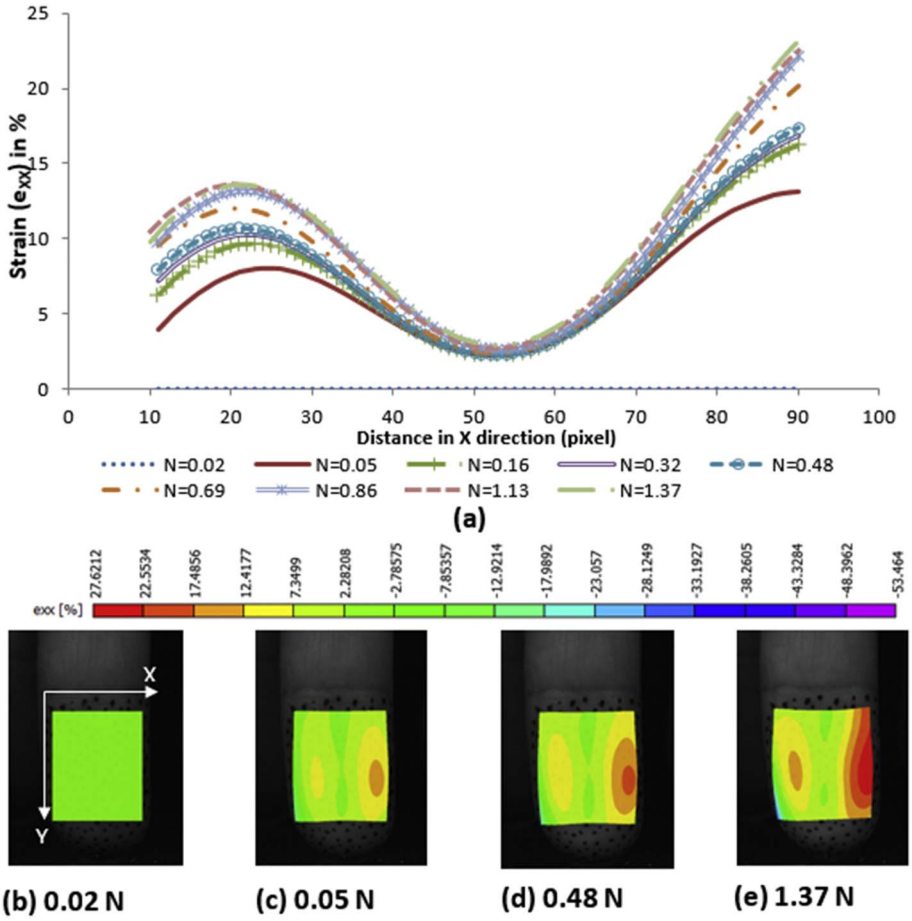

Fig. 9. (a) Percentage strain (e_{xx}) on finger-pad skin at different position in static phase with negligible shear force; (b–e) four examples of corresponding DIC images.

tangential forces acting on the mid-region of the finger in the pre-loading phase (P_{12}). During the dynamic phase, the strain in the mid region is still relatively small approximately 1%.

The contact in the middle region plays a less important role in finger-pad friction, compared to the edges as shown in Fig. 11. During initial contact, DIC images of finger show that the middle region of the finger-pad was in contact with the glass surface. This region, referred to as the 'stick' zone, was sticking to the glass plate, whereas, other regions moved with the finger during the transition phase. The magnitude of strain in the X-axis (Fig. 10, P1 to P37) is lowest in the middle region (red dotted line in Fig. 11) compared to the edges indicating that the influence of sliding interactions in this region will also be lowest. A similar experiment to determine the contact area [29] reported a decrease in contact area with an increase in tangential force when the finger starts sliding. This signifies that the real contact area decreases suggesting that the middle regions in the X and Y axes do not play a major role in sliding interactions, compared to the edge regions. The trailing edge in the imaged region underwent significant deformation after the finger overcame the interface resistance, on the verge of moving. This region can be defined as the 'slip' zone. During continuous sliding, the stick zone gradually converted to the slip.

Similar studies by André et al. [14] and Terekhov and Hayward [25] have showed that with increasing friction force, the stick region decreased under the action of constant load. In the current study, the stick region decreased as the friction force increased from 0 (at P_1) to 1.79 N (at P_{12}). No presence of stick region was observed for points P_{16} and P_{37} due to the conversion of stick region to slip. The process follows in portions of skin adhering (stuck) while other regions slipped. This

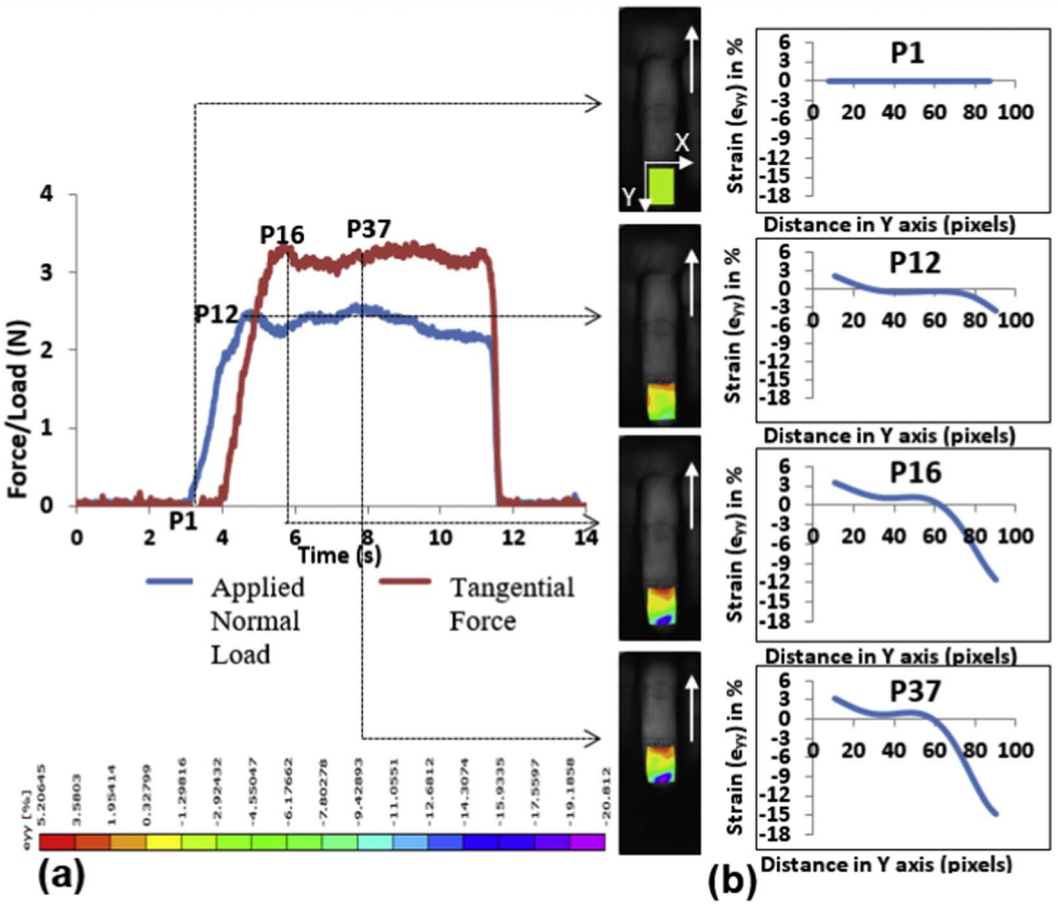

Fig. 10. (a) Applied normal load and tangential force plots as a function of time; (b) Strain field and percentage strain (e_{yy}) at four different data points (P1, P12, P16, P37) with compressive (positive) and tensile (negative) strains. The arrow in the strain field represents the movement of finger with respect to glass. The 0 displacement is at the interphalengeal joint.

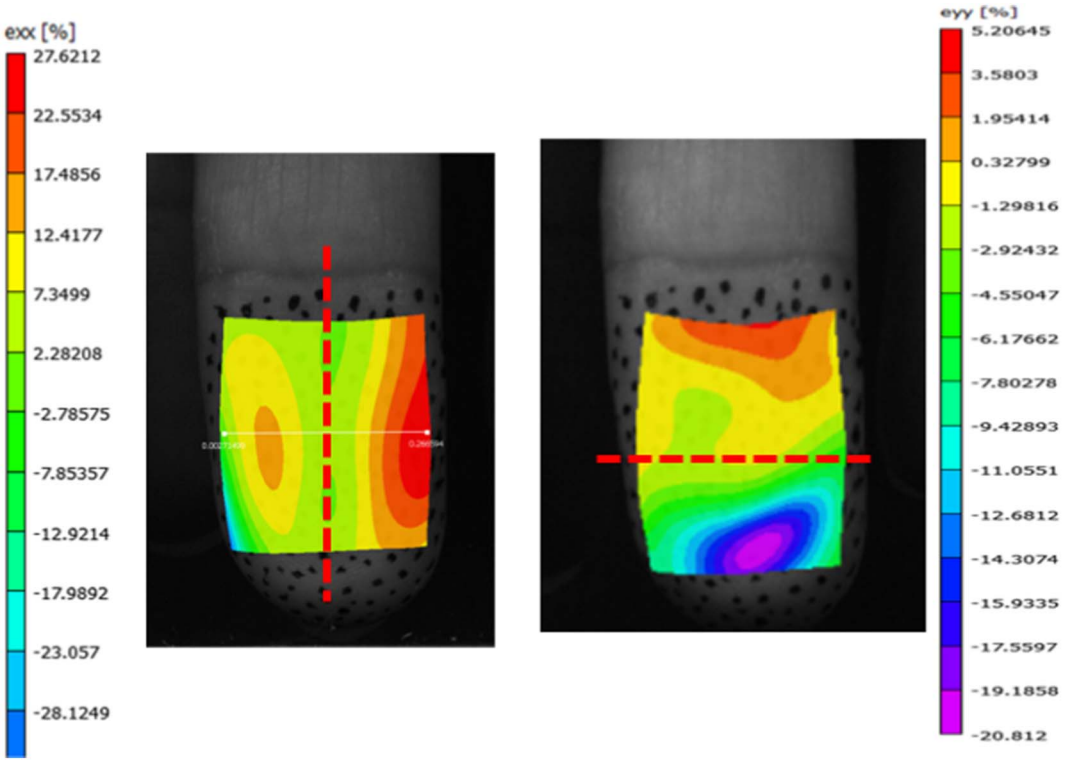

Fig. 11. Strain fields in the X and Y axes. The red dotted lines signify the regions of minimum strain. (For interpretation of the references to colour in this figure legend, the reader is referred to the web version of this article.)

evolution of contact state has been termed partial slip [30–31]. During partial slip, the outer periphery of the finger-pad showed higher strain similar to reported in Delhaye et al. [23]. However, the magnitude and direction of the strain cannot be compared as the sliding direction of glass in their study was perpendicular to the sliding direction of finger adapted in the current study. Due to limitation on the speed of DIC and OCT, images were captured only at partial slip and stick region. A detail investigation on the contact area during static and dynamic phase will give further information on the real area when is in contact with glass surface. This information will be useful when designing elastography equipment as suggested in Hu et al. [32].

4. Conclusions

A new technique to evaluate the mechanical properties, such as strain of skin, was developed using OCT and DIC. Strain was measured at different stages of sliding. Slip and stick regions were seen during static phase and stick region converted to slip during dynamic phase due to sliding of the finger against the surface. There is a lack of contact observed in the middle region of the finger concluding that no force is acting in the middle region during sliding. This implies that different regions of finger-pad behave differently during static and dynamic phases.

This case study was performed on only one subject. Further studies with more subjects are needed to observe whether the same behaviour is replicated on others. This will also implicate the variation of skin properties among different subjects (stratification) due to variation of thickness, roughness, geometry [33], melanin and erythema content.

Acknowledgements

The research was supported in part by Chinese Scholarship Council and Engineering and Physical Science Research Council (EP/K009699/1).

References

[1] K.S. Saladin, The integumentary system, Human Anatomy, McGraw-Hill, New York, 2008, pp. 128–152.
[2] M. Geerligs, General information, Skin Layer Mechanics, Universiteitsdrukkerij TU Eindhoven, Eindhoven, 2009, pp. 1–14.
[3] E. Baussan, M.A. Bueno, R.M. Rossi, S. Derler, Analysis of current running sock structures with regard to blister prevention, Text. Res. J. 83 (2012) 836–848.
[4] A.B. Cua, K.P. Wilhelm, H.I. Maibach, Frictional properties of human skin: relation to age, sex and anatomical region, stratum corneum hydration and transepidermal water loss, Br. J. Derm. 123 (4) (1990) 473–479.
[5] P. Elsner, D. Wilhelm, H.I. Maibach, Frictional properties of human forearm, and vulvar skin: influence of age and correction with transepidermal water loss and capacitance, Dermatologica 181 (2) (1990) 88–91.
[6] J. Asserin, H. Zahouani, P.H. Humbert, V. Couturaud, D. Mougin, Measurement of the friction coefficient of the human skin in vivo. Quantification of the cutaneous smoothness, Colloids Surf. B: Biointerfaces 19 (2000) 1–12.
[7] S. Derler, L.-C. Gerhardt, Tribology of skin: review and analysis of experimental results for the friction coefficient of human skin, Tribol. Lett. 45 (1) (2012) 1–27.
[8] S.E. Tomlinson, R. Lewis, M.J. Carré, The effect of normal force and roughness on friction in human finger contact, Wear 267 (5–8) (2009) 1311–1318.
[9] M.A. Darden, C.J. Schwartz, Investigation of skin tribology and its effect on the tactile attributes of polymer fabrics, Wear 267 (2009) 1289–1294.
[10] C.P. Hendriks, S.E. Franklin, Influence of surface roughness material and climate conditions on the friction of human skin, Tribol. Lett. 37 (2010) 361–373.
[11] O. Bobjer, S.E. Johansson, S. Piguet, Friction between hand and handle. Effects of oil and lard on textured and non textured surfaces; perception of discomfort, Appl. Ergon. 24 (3) (1993) 190–202.
[12] S.E. Tomlinson, R. Lewis, X. Liu, C. Texier, M.J. Carré, Understanding the friction mechanisms between the human finger and flat contacting surfaces in moist conditions, Tribol. Lett. 41 (1) (2011) 283–294.
[13] M.J. Adams, S.A. Johnson, P. Lefèvre, V. Lévesque, V. Hayward, T. André, J.-L. Thonnard, Finger pad friction and its role in grip and touch, J. R. Soc. Interface 10 (2013) 20120467, http://dx.doi.org/10.1098/rsif.2012.0467.
[14] T. André, V. Lévesque, V. Hayward, P. Lefèvre, J.-L. Thonnard, Effect of skin hydration on the dynamics of fingertip gripping contact, J. R. Soc. Interface 8 (64) (2011) 1574–1583.
[15] A. Ní Annaidh, K. Bruyère, M. Destrade, M.D. Gilchrist, M. Otténio, Characterization of the anisotropic mechanical properties of excised human skin, J. Mech. Behav. Biomed. Mater. 5 (1) (2012) 139–148.
[16] M. Ottenio, D. Tran, A. Ní Annaidh, M.D. Gilchrist, K. Bruyère, Strain rate and anisotropy effects on the tensile failure characteristics of human skin, J. Mech. Behav. Biomed. Mater. 41 (2015) 241–250.
[17] K. Genovese, A. Montes, A. Martinez, S.L. Evans, Full-surface deformation measurement of anisotropic tissues under indentation, Med. Eng. Phys. 37 (5) (2015) 484–493.
[18] J.-S. Affagard, P. Feissel, S.F. Bensamoun, Measurement of the quadriceps muscle displacement and strain fields with ultrasound and Digital Image Correlation (DIC) techniques, IRBM 36 (3) (2015) 170–177.
[19] J. Enfield, E. Jonathan, M. Leahy, In vivo imaging of the microcirculation of the volar forearm using correlation mapping optical coherence tomography (cmOCT), Biomed. Opt. Express 2 (5) (2011) 1184–1193.
[20] T. Gambichler, A. Pljakic, L. Schmitz, Recent advances in clinical application of optical coherence tomography of human skin, Clin. Cosmet. Investig. Dermatol. 8 (2015) 345–354.
[21] Y. Zhang, G. Wu, H. Wei, Z. Guo, H. Yang, Y. He, S. Xie, Y. Liu, Continuous non-invasive monitoring of changes in human skin optical properties during oral intake of different sugars with optical coherence tomography, Biomed. Opt. Express 5 (4) (2014) 990–999.
[22] X. Liu, Z. Lu, R. Lewis, M.J. Carré, S.J. Matcher, Feasibility of using optical coherence tomography to study the influence of skin structure on finger friction, Tribol. Int. 63 (2013) 34–44.
[23] B. Delhaye, A. Barrea, B.B. Edin, P. Lefèvre, J.-T. Thonnard, Surface strain measurements of fingertip skin under shearing, J. R. Soc. Interface 13 (2016) 20150874.
[24] M. Tada, T. Kanade, An imaging system of incipient slip for modelling how human perceives slip of a fingertip, Conf. Proc. IEEE Eng. Med. Biol. Soc. (2004) 2045–2048.
[25] A.V. Terekhov, V. Hayward, Minimal adhesion surface area in tangentially loaded digital contacts, J. Biomech. 44 (13) (2011) 2508–2510.
[26] A.F. Fercher, W. Drexler, C.K. Hitzenberger, T. Lasser, Optical coherence tomography-principles and applications, Rep. Prog. Phys. 66 (2) (2003) 239–303.
[27] M.A. Sutton, W.J. Wolters, W.H. Peters, W.F. Ranson, S.R. McNeill, Determination of displacements using an improved digital correlation method, Image Vis. Comput. 1 (3) (1983) 133–139.
[28] R. Maiti, L.-C. Gerhardt, Z.S. Lee, R.A. Byers, D. Woods, J.A. Sanz-Herrera, S.E. Franklin, R. Lewis, S.J. Matcher, M.J. Carré, In vivo measurement of skin surface strain and sub-surface layer deformation induced by natural tissue stretching, J. Mech. Behav. Biomed. Mater. 62 (2016) 556–569.
[29] X. Liu, M.J. Carré, Q. Zhang, Z. Lu, S.J. Matcher, R. Lewis, Measuring contact area in a sliding human finger-pad contact, Skin Res. Technol. 00 (2017) 1–14, http://dx.doi.org/10.1111/srt.12387.
[30] H. Kinoshita, L. Bäckström, J.R. Flanagan, R.S. Johansson, Tangential torque effects on the control of grip forces when holding objects with a precision grip, J. Neurophysiol. 78 (3) (1997) 1619–1630.
[31] T. Soneda, K. Nakano, Investigation of vibrotactile sensation of human fingerpads by observation of contact zones, Tribol. Int. 43 (2010) 210–217.
[32] X. Hu, R. Maiti, J. Boadi, W. Li, M.J. Carré, R. Lewis, S. Franklin, S.J. Matcher, Optical coherence elastography for human finger-pad skin deformation studies, SPIE Proc 9710, Optical Elastography and Tissue Biomechanics III, 97100C, March 9, 2016.
[33] M.A. Srinivasan, R.J. Gulati, K. Dandekar, In vivo compressibility of the human fingertip, in: M.W. Bidez (Ed.), Advances in Bioengineering, 8–13 American Society of Mechanical Engineers, New York, NY, November 1992, pp. 291–394 (ASME Annual Winter Meeting, Anaheim, CA).